

Interaction-induced exotic vortex states in an optical lattice clock with spin-orbit coupling

Xiaofan Zhou,^{1,2} Jian-Song Pan,^{3,4,5} Wei Yi,^{3,4,*} Gang Chen,^{1,2,†} and Suotang Jia^{1,2}

¹State Key Laboratory of Quantum Optics and Quantum Optics Devices,
Institute of Laser Spectroscopy, Shanxi University, Taiyuan 030006, China

²Collaborative Innovation Center of Extreme Optics,
Shanxi University, Taiyuan, Shanxi 030006, China

³Key Laboratory of Quantum Information, University of Science and Technology of China, CAS, Hefei, Anhui, 230026, China

⁴Synergetic Innovation Center of Quantum Information and Quantum Physics,
University of Science and Technology of China, Hefei, Anhui 230026, China

⁵Wilczek Quantum Center, School of Physics and Astronomy and T. D. Lee Institute,
Shanghai Jiao Tong University, Shanghai 200240, China

Motivated by a recent experiment [L. F. Livi, *et al.*, Phys. Rev. Lett. **117**, 220401(2016)], we study the ground-state properties of interacting fermions in a one-dimensional optical lattice clock with spin-orbit coupling. As the electronic and the hyperfine-spin states in the clock-state manifolds can be treated as effective sites along distinct synthetic dimensions, the system can be considered as multiple two-leg ladders with uniform magnetic flux penetrating the plaquettes of each ladder. As the inter-orbital spin-exchange interactions in the clock-state manifolds couple individual ladders together, we show that exotic interaction-induced vortex states emerge in the coupled-ladder system, which compete with existing phases of decoupled ladders and lead to a rich phase diagram. Adopting the density matrix renormalization group approach, we map out the phase diagram, and investigate in detail the currents and the density-density correlations of the various phases. Our results reveal the impact of interactions on spin-orbit coupled systems, and are particularly relevant to the on-going exploration of spin-orbit coupled optical lattice clocks.

I. INTRODUCTION

Spin-orbit coupling (SOC) plays a key role in solid-state topological materials such as topological insulators and quantum spin Hall systems [1–3]. The experimental realization of synthetic SOC in cold atomic gases opens up the avenue of simulating synthetic topological matter on the versatile platform of cold atoms [4–18]. In most of the previous studies, synthetic SOC is typically implemented in alkali atoms using a two-photon Raman process, in which different spin states in the ground-state hyperfine manifold of the atoms are coupled. Thus, as the atoms undergo Raman-assisted spin flips, their center-of-mass momenta also change due to the photon recoil. Alternatively, by considering the atomic spin states as discrete lattice sites, the SOC can also be mapped to effective tunneling in the so-called synthetic dimension [19–22]. Such an interpretation has led to the realization of two-leg ladder models with synthetic magnetic flux, and to the subsequent experimental demonstration of chiral edge states using cold atoms [10, 23, 24].

For systems under the synthetic SOC generated by the Raman scheme, a key experimental difficulty in reaching the desired many-body ground states is the heating caused by high-lying excited states in the Raman process, whose single-photon detuning is limited by the fine-structure splitting [4–6]. This problem can be over-

come either by choosing atomic species with large fine-structure splitting [25, 26], or by using alkaline-earth-like atoms [27], which feature long-lived excited states. Indeed, in two recent experiments, synthetic SOC with significantly reduced heating have been experimentally demonstrated by directly coupling the ground 1S_0 (referred to as $|g\rangle$) and the metastable 3P_0 (referred to as $|e\rangle$) clock-state manifolds of ^{87}Sr or ^{173}Yb lattice clocks [10, 11]. In Ref. [10], the electronic states are further mapped onto the effective lattice sites along a synthetic dimension, such that a two-leg ladder model with uniform magnetic flux is realized and the resulting chiral edge currents are probed. Similar models for bosonic systems have been extensively investigated in the past [28–35]. When the flux is small, chiral edge currents emerge at the system boundary, where the currents along the two legs are opposite in direction. This is reminiscent of the Meissner effects of superconductivity [36]. When the flux becomes sufficiently large, the system undergoes a phase transition as the chiral edge currents are replaced by vortex lattices in the bulk, where currents exist on both the rungs and the edges of the ladder.

Furthermore, when taking the hyperfine spin states in the clock-state manifolds into account, one can map both the electronic and the spin degrees of freedom into distinct synthetic dimensions, such that the system in Ref. [10] can be extended to model multiple two-leg ladders with synthetic magnetic flux penetrating the plaquettes of each ladder. Here, different electronic states label the two legs of each ladder, and different spin states label different ladders. It would then be interesting to study the ground state of the system as the parame-

*Electronic address: wyz@ustc.edu.cn

†Electronic address: chengang971@163.com

ters such as the flux or the interactions are tuned. In the clock-state manifolds of alkaline-earth-like atoms, the nuclear and the electronic degrees of freedom are separated, and the short-range two-body interactions occur either in the electronic spin-singlet channel $|-\rangle = \frac{1}{2}(|ge\rangle - |eg\rangle) \otimes (|\downarrow\uparrow\rangle + |\uparrow\downarrow\rangle)$, or in the electronic spin-triplet channel $|+\rangle = \frac{1}{2}(|ge\rangle + |eg\rangle) \otimes (|\downarrow\uparrow\rangle - |\uparrow\downarrow\rangle)$ [37–39]. Here, $|\uparrow\rangle$ and $|\downarrow\rangle$ label different spin states in the $|g\rangle$ or $|e\rangle$ hyperfine manifolds. As reported in previous studies, such an inter-orbital spin-exchange interaction would induce density-ordered states in either the spin or the charge channel, leading to spin-density wave (SDW), orbital-density order (ODW) or charge-density wave (CDW) phases [40–48]. More interestingly, these interactions would couple the otherwise independent ladders, which may induce new patterns of current flow in the system.

In this work, adopting the concept of synthetic dimensions, we explicitly consider the hyperfine spin states in the clock-state manifolds and map the system in Ref. [10] to multiple two-leg ladders (see Fig. 1). Using the density matrix renormalization group (DMRG) approach [49, 50], we then numerically investigate the effect of interactions on the many-body ground-state properties such as the current flow and the density-density correlations. Our numerical results reveal a rich phase diagram, where the interactions drastically modify the Meissner and the vortex states in the non-interacting case. In particular, we show the existence of an exotic interaction-induced vortex state, where spin currents emerge between different ladders together with SDW in the system. As the interactions in the clock-state manifolds can be readily tuned by external magnetic field through the orbital Feshbach resonance [51–53], or by transverse trapping frequencies through the confinement-induced resonance [54, 55], our results have interesting implications for future experiments.

The work is organized as follows. In Sec. II, we present the system setup and the mode Hamiltonian. We discuss the phase diagram of the non-interacting case in Sec. III. We then study in detail the impact of interactions on the Meissner state and the vortex state, respectively in Secs. IV and V. The detection and conclusion are given respectively in Secs. VI and VII.

II. MODEL AND HAMILTONIAN

We consider a similar setup as in the recent experiment on synthetic SOC in optical lattice clocks [10]. As shown in Fig. 1(a), a pair of counter-propagating laser with the “magic” wavelength $\lambda_L = 2\pi/k_L$ is used to generate a one-dimensional (1D) optical lattice potential $V_L(x) = V_x \cos^2(k_L x)$, where V_x is the lattice depth. The synthetic SOC is implemented by an ultra-narrow π -polarized clock laser with a wavelength λ_C , which drives a single-photon transition between the clock states with the same nuclear

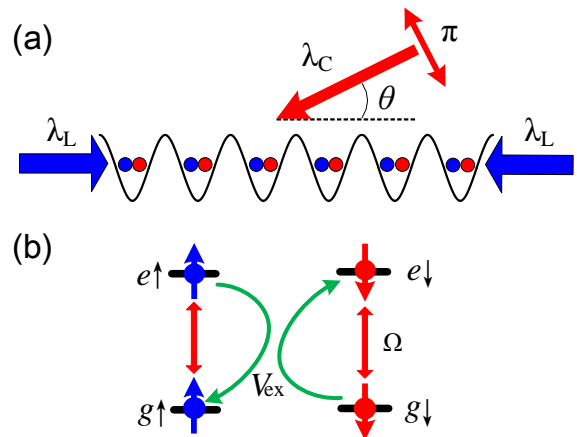


FIG. 1: (a) Schematics of the experimental setup. The ultracold alkaline-earth-like atoms are trapped in a 1D optical lattice, which is generated by a pair of counter-propagating lasers with the “magic” wavelength λ_L , such that states in the clock-state manifolds 1S_0 and 3P_0 are subject to the same lattice potential. An ultranarrow π -polarized clock laser with a wavelength λ_C drives a single-photon transition between the clock-state manifolds. By introducing an angle θ between the clock laser and that generating the optical lattice, the photon recoil momentum becomes $k_C = 2\pi \cos\theta/\lambda_C$ and can be tuned experimentally. (b) Energy levels considering two nuclear spin states $|\uparrow\rangle$ and $|\downarrow\rangle$ in each manifold. While states in the 1S_0 and 3P_0 manifolds are coherently coupled by the spin-conserving clock laser (the red curves), the interaction in the clock-state manifolds can couple distinct spin states in different orbitals (the green curves).

spins. Due to the existence of the angle θ between the wave vector of the clock laser and the alignment of the 1D optical lattice [see Fig. 1(a)], the momentum transfer becomes $k_C = 2\pi \cos\theta/\lambda_C$ [10]. A key ingredient in this system is the inter-orbital spin-exchange interaction [37–39], as shown by the green curves in Fig. 1(b). The full Hamiltonian is written as ($\hbar = 1$ hereafter)

$$\hat{H}_T = \hat{H}_L + \hat{H}_C + \hat{H}_I \quad (1)$$

with

$$\hat{H}_L = \sum_{\alpha\sigma} \int dx \hat{\psi}_{\alpha\sigma}^\dagger(x) \left[-\frac{\nabla^2}{2m} + V_L(x) \right] \hat{\psi}_{\alpha\sigma}(x), \quad (2)$$

$$\hat{H}_C = \frac{\Omega_R}{2} \sum_{\sigma} \int dx [\hat{\psi}_{g\sigma}^\dagger(x) e^{ik_C x} \hat{\psi}_{e\sigma}(x) + \text{H.c.}], \quad (3)$$

$$\begin{aligned} \hat{H}_I = & \frac{g_{\pm}}{2} \int dx [\Psi_{g\uparrow}^\dagger \Psi_{e\downarrow}^\dagger \mp \Psi_{g\downarrow}^\dagger \Psi_{e\uparrow}^\dagger] [\Psi_{e\downarrow} \Psi_{g\uparrow} \mp \Psi_{e\uparrow} \Psi_{g\downarrow}] \\ & + g_- \int dx [\Psi_{g\uparrow}^\dagger \Psi_{e\uparrow}^\dagger \Psi_{e\uparrow} \Psi_{g\uparrow} + \Psi_{g\downarrow}^\dagger \Psi_{e\downarrow}^\dagger \Psi_{e\downarrow} \Psi_{g\downarrow}], \quad (4) \end{aligned}$$

where $\alpha = \{g, e\}$ is the orbit index, $\sigma = \{\uparrow, \downarrow\}$ is the spin index, $\Psi_{\alpha\sigma}$ and $\Psi_{\alpha\sigma}^\dagger$ are the corresponding field operators, Ω_R is the Rabi frequency of the clock laser, g_{\pm}

are the 1D interaction strengths [51, 55], and H.c. is the Hermitian conjugate. Note that in writing down Hamiltonian (1), we only consider four nuclear spin states from the $|g\rangle$ and $|e\rangle$ manifolds. In principle, the other nuclear spin states can be shifted away by imposing spin-dependent laser shifts [24].

When the 1D optical lattice is deep enough and Ω_R is not too large [56–58], we may take the single-band approximation and write down the corresponding tight-binding model

$$\begin{aligned} \hat{H}_{\text{TB}} = & -t \sum_{\langle i,j \rangle, \alpha\sigma} \hat{c}_{i\alpha\sigma}^\dagger \hat{c}_{j\alpha\sigma} + \frac{\Omega}{2} \sum_{j,\sigma} (e^{i\phi j} \hat{c}_{jg\sigma}^\dagger \hat{c}_{je\sigma} + \text{H.c.}) \\ & + U \sum_j (\hat{n}_{jg\uparrow} \hat{n}_{je\downarrow} + \hat{n}_{jg\downarrow} \hat{n}_{je\uparrow}) + U_0 \sum_{j\sigma} \hat{n}_{jg\sigma} \hat{n}_{je\sigma} \\ & + V_{\text{ex}} \sum_j (\hat{c}_{jg\uparrow}^\dagger \hat{c}_{je\downarrow}^\dagger \hat{c}_{je\uparrow} \hat{c}_{jg\downarrow} + \text{H.c.}), \end{aligned} \quad (5)$$

where $\hat{c}_{j\alpha\sigma}$ ($\hat{c}_{j\alpha\sigma}^\dagger$) is the annihilation (creation) operator for atoms on the i th site of the α orbital and the spin σ , $\hat{n}_{j\alpha\sigma} = \hat{c}_{j\alpha\sigma}^\dagger \hat{c}_{j\alpha\sigma}$. The spin-conserving hopping rate $t = \left| \int dx w^{(j)} \left[-\frac{\nabla^2}{2m} + V_L(x) \right] w^{(j+1)} \right|$, with $w^{(j)}$ being the lowest-band Wannier function on the j th site of the lattice potential $V_L(x)$. The spin-flipping hopping rate $\Omega = \Omega_R \int dx w^{(j)} e^{ik_C x} w^{(j)}$. $\phi = \frac{1}{2} k_C \lambda_L = \pi \lambda_L \cos \theta / \lambda_C$ is the synthetic magnetic flux per plaquette induced by the SOC, $U = \frac{1}{2} (g_+ + g_-) \int dx w^{(j)} w^{(j)} w^{(j)} w^{(j)}$ and $U_0 = g_- \int dx w^{(j)} w^{(j)} w^{(j)} w^{(j)}$ are the inter-orbital density-density interaction strengths with the same and different nuclear spins, respectively. $V_{\text{ex}} = \frac{1}{2} (g_- - g_+) \int dx w^{(j)} w^{(j)} w^{(j)} w^{(j)}$ is the inter-orbital spin-exchange interaction strength. Hamiltonian (5) has the advantage that all parameters can be tuned independently. For example, t can be controlled by the depth of the optical lattice potential, Ω and ϕ can be controlled by the Rabi frequency and the angle of the clock laser, respectively, and $\{V_{\text{ex}}, U, U_0\}$ can be tuned through the orbital Feshbach resonance [51–53] or the confinement induced resonance [54, 55]. In the following, we take $U_0 = V_{\text{ex}} + U$, which is dictated by the scattering parameters of ^{173}Yb atoms [54, 55].

From the tight-binding Hamiltonian (5), it is clear that if we drop the interaction terms and map the electronic (α) and the spin (σ) states onto effective lattice sites along two different synthetic dimensions, the non-interacting tight-binding model describes a pair of two-leg ladders. We label the two synthetic dimensions as the orbit α - and the spin σ -directions, respectively, while the optical lattice lies along the x -direction. We may then denote the synthetic dimensions as SD α and SD σ , respectively. As illustrated in Fig. 2, the pair of ladders each lie within the (x, α) plane with the legs of both ladders along the x -direction. The rung tunneling in each ladder is facilitated by the SOC, which also induces uniform magnetic flux in each plaquette of the ladder. In the absence of interactions, the ladders are

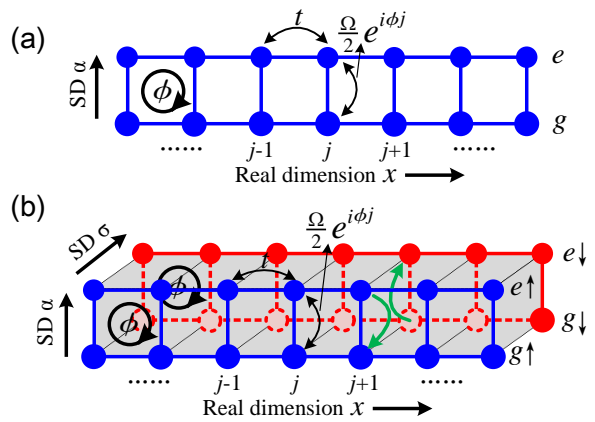


FIG. 2: (a) A two-leg synthetic ladder with a synthetic magnetic flux $\phi = \pi \lambda_L / \lambda_C \cos \theta$ in each plaquette. The orbital states can be treated as an effective synthetic dimension denoted as SD α . The two ladders along the synthetic dimension SD σ are identical and decoupled. (b) A pair of two-leg synthetic ladders (i.e., $|g \uparrow, e \uparrow\rangle$ and $|g \downarrow, e \downarrow\rangle$), with the same flux, are coupled by the inter-orbital spin-exchange interaction (green curves). In this lattice, there are two-direction synthetic dimensions, SD α and SD σ .

not coupled, as different spin states are independent on the single-body level. However, the inter-orbital spin-exchange interaction effectively couples the ladders together [see Fig. 2(b)], which, as we will show later, induce inter-ladder currents along the σ -direction.

An important property here is the current along the legs and the rungs of the ladder. Local and average currents along the x -direction can be defined as [29, 30, 59],

$$J_{j,\alpha\sigma}^{\parallel} = i \left(\hat{c}_{j+1\alpha\sigma}^\dagger \hat{c}_{j\alpha\sigma} - \hat{c}_{j\alpha\sigma}^\dagger \hat{c}_{j+1\alpha\sigma} \right), \quad (6)$$

$$J_{\alpha\sigma}^{\parallel} = \frac{1}{L} \sum_j J_{j,\alpha\sigma}^{\parallel}. \quad (7)$$

Similarly, currents along the α -direction can be defined as [30],

$$J_{j,\alpha}^{\perp} = i (e^{i\phi j} \hat{c}_{je\sigma}^\dagger \hat{c}_{jg\sigma} - e^{-i\phi j} \hat{c}_{jg\sigma}^\dagger \hat{c}_{je\sigma}), \quad (8)$$

$$J_{\alpha}^{\perp} = \frac{1}{L} \sum_j |J_{j,\alpha}^{\perp}|, \quad (9)$$

Finally, we also define currents along the σ -direction as

$$J_{j,\sigma}^{\perp} = i (\hat{c}_{j\alpha\downarrow}^\dagger \hat{c}_{j\alpha\uparrow} - \hat{c}_{j\alpha\uparrow}^\dagger \hat{c}_{j\alpha\downarrow}), \quad (10)$$

$$J_{\sigma}^{\perp} = \frac{1}{L} \sum_j |J_{j,\sigma}^{\perp}|. \quad (11)$$

In the following discussions, we adopt the DMRG formalism to calculate the ground state of the system, from which we characterize currents and density correlation functions. For the numerical calculation, we have considered length of chain L up to 32 sites. We keep

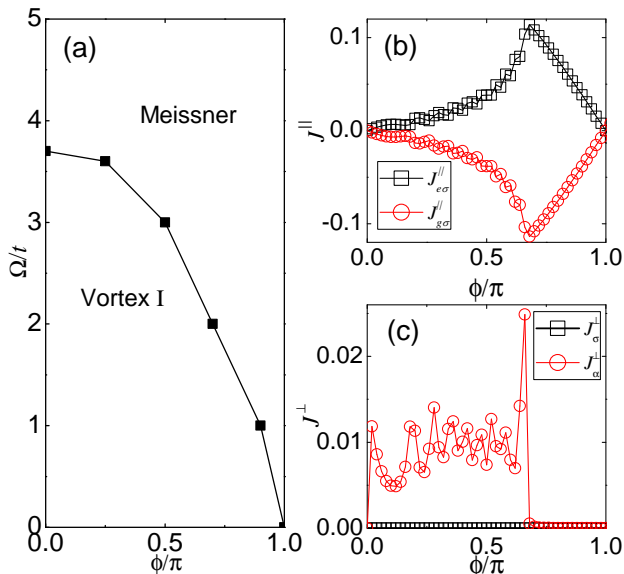


FIG. 3: (a) Phase diagram in the (Ω, ϕ) plane. The currents (b) J^{\parallel} and (c) J^{\perp} as functions of ϕ/π . In all subfigures, $U = U_0 = V_{\text{ex}} = 0$ and $n = 1$, and (b) and (c) have the other parameter $\Omega/t = 2$.

the maxstates $m = 200$ and achieve truncation errors of 10^{-10} . We mainly consider the case of half filling, i.e., $n = N/(2L) = 1$, where L is the length of chain and N is the total number of atoms.

III. PHASES AND CURRENTS IN THE NON-INTERACTING CASE

We first discuss the ground-state phases of the system in the absence of interactions. In this case, different spin states are decoupled, and we may identify a pair of two-leg ladders, as illustrated in Fig. 2. From our numerical calculations, we find that only the Meissner and the vortex states appear in the ground-state phase diagram shown in Fig. 3(a). Typically, when the synthetic flux is small, the ground state is the so-called Meissner state, where the edge currents $J_{g\sigma}^{\parallel}$ and $J_{e\sigma}^{\parallel}$ flow in opposite directions along the two legs of each ladder [10, 23, 29], as shown in Fig. 3(b). Upon increasing the flux above a critical value, the ground state features a vortex state with rung currents and vortex lattice structures in the bulk of each ladder, i.e., in the (x, α) plane. The existence of this so-called Vortex I state is confirmed in Fig. 3(c), where nonzero J_{α}^{\perp} in the Vortex I state regime indicates a finite current along the rungs in the α -direction for each ladder. The current J_{σ}^{\perp} remains zero in the non-interacting case, which is consistent with the picture of two independent ladders of different spins. We also note that in the non-interacting case, there are

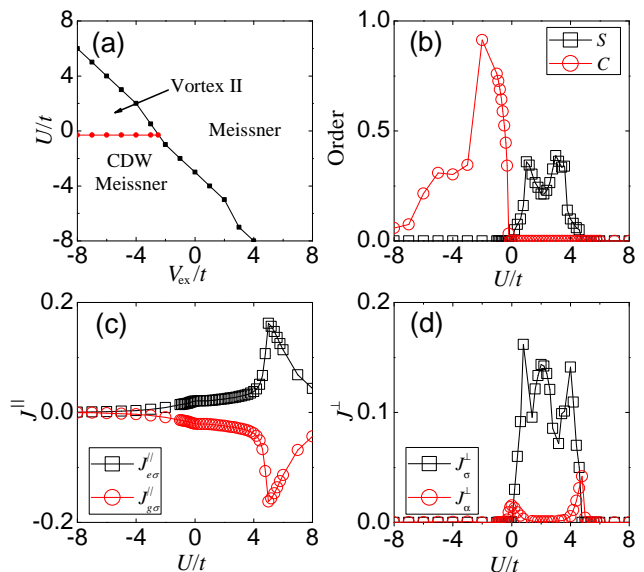


FIG. 4: (a) Phase diagram in the (U, V_{ex}) plane. (b) The SDW order S and the CDW order C as well as the currents (c) J^{\parallel} and (d) J^{\perp} as functions of U/t . In all subfigures, $\Omega/t = 4$, $\phi/\pi = 0.75$, and $n = 1$, and (b)-(d) have the other parameter $V_{\text{ex}}/t = -6$.

no density-ordered phases.

IV. IMPACT OF INTERACTIONS ON THE MEISSNER STATE

We now study the impact of interactions on the Meissner state for $\Omega/t = 4$ and $\phi/\pi = 0.75$. As the interactions are turned on, the system can undergo phase transitions into exotic vortex states or phases with density orders. We map out the phase diagram in the (U, V_{ex}) plane, while fixing other parameters. As shown in Fig. 4(a), the phase diagram consists of three different phases: a simple Meissner state, a Meissner state with CDW, and an exotic vortex state with SDW, which we label as Vortex II state. The simple Meissner state resembles the Meissner state in the non-interacting case with chiral edge currents and no density-orders in the bulk. The CDW Meissner state features chiral edge currents as well as finite CDW density correlations in the bulk. The most interesting state here is the Vortex II state, which features finite SDW correlations as well as currents and vortex lattice structures in the (x, σ) plane.

The phase boundaries between these phases can be determined from the CDW and the SDW correlations, as well as from the currents' calculations. As illustrated in Fig. 4(b), for a fixed $V_{\text{ex}}/t = -6$, the CDW order

$$C = \frac{1}{2L} \sum_j (-1)^j n_j \quad (12)$$

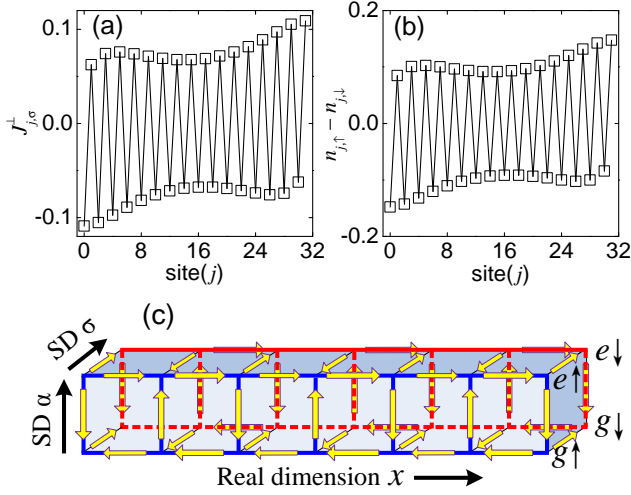


FIG. 5: (a) The currents J^\perp and (b) density profiles $n_{j,\uparrow} - n_{j,\downarrow}$ for different sites. (c) Sketch of currents of the Vortex II state. In (a) and (b), $\Omega/t = 4$, $\phi/\pi = 0.75$, $V_{\text{ex}}/t = -6$, $U/t = 2$, and $n = 1$.

has a finite value in the range $-8 < U/t < 0$, while the SDW order

$$S = \frac{1}{L} \sum_j (-1)^j (n_{j,\uparrow} - n_{j,\downarrow}) \quad (13)$$

has a finite value for $0 < U/t < 4.7$. On the other hand, while the edge currents $J_{\alpha\sigma}^\parallel$ are always finite and opposite in directions for different sites in the α direction, the currents J_σ^\perp and J_α^\perp only exist within a range, as shown in Figs. 4(c) and 4(d). In particular, the non-vanishing J_σ^\perp indicates inter-ladder currents and vortices in the (x, σ) plane. To further characterize the Vortex II state, in Figs. 5(a) and 5(b), we show the spatial distribution of the inter-ladder currents as well as the spin density. Apparently, the SDW and the vortex lattice structure in the (x, σ) plane is due to the interplay of the inter-orbital spin-exchange interaction and the synthetic magnetic flux in the (x, α) plane, as shown in Fig. 5(c).

V. IMPACT OF INTERACTIONS ON THE VORTEX STATE

In this section, we study the impact of interactions on the vortex states. In Fig. 6, we map out the phase diagram in the (U, V_{ex}) plane for $\Omega/t = 2$ and $\phi/\pi = 0.25$. In the absence of interactions, the system is in the vortex state. With interactions, the system can undergo phase transitions into various different phases. As shown in Fig. 6(a), besides the Vortex II state and the CDW Meissner state, several other exotic phases emerge in the

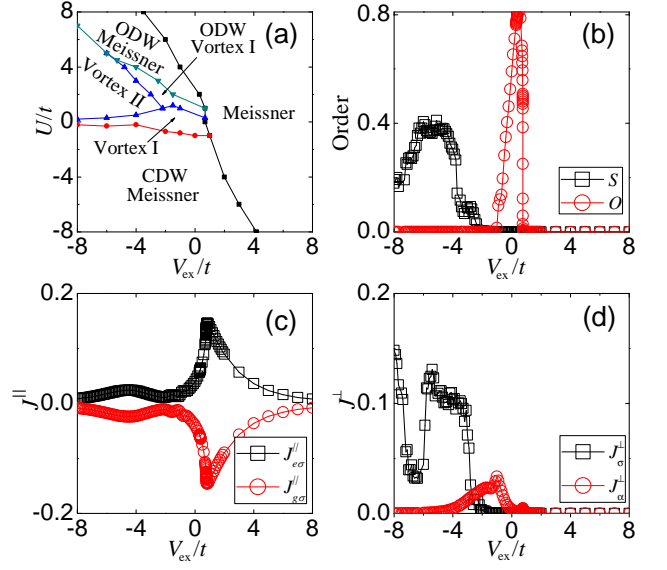


FIG. 6: (a) Phase diagram in the (U, V_{ex}) plane. (b) The SDW order S and the ODW order O as well as the currents (c) J^\parallel and (d) J^\perp as functions of V_{ex}/t . In all subfigures, $\Omega/t = 2$, $\phi/\pi = 0.25$, and $n = 1$, and (b)-(d) have the other parameter $U/t = 1$.

phase diagram. While the Vortex I resembles the vortex state in the absence of interactions, interesting phases with density correlations in the orbital channel appear, which can be further differentiated by their currents flows as the ODW Meissner state and the ODW Vortex I state, where the vortex occurs in the (x, α) plane, together with density-wave orders in the orbital channel. Here the ODW order is defined as

$$O = \frac{1}{L} \sum_j (-1)^j (n_{j,g} - n_{j,e}). \quad (14)$$

In Figs. 6(b)-6(d), we plot the currents and the density wave orders as functions of V_{ex}/t for $U/t = 1$. For $V_{\text{ex}}/t \in [-8, -2.06]$, the SDW order S has a finite value, the ODW order vanishes with $O = 0$, the currents $J_{\alpha\sigma}^\parallel > 0$ and $J_\sigma^\perp > 0$, the corresponding phase is the Vortex II state. When $V_{\text{ex}}/t \in [-2.06, -1]$, the SDW order $S = 0$, the ODW order $O = 0$, the currents $J_{\alpha\sigma}^\parallel > 0$, $J_\alpha^\perp > 0$, and $J_\sigma^\perp = 0$, the corresponding phase is the Vortex I state. When $V_{\text{ex}}/t \in [-1, 0.77]$, the SDW order $S = 0$, the ODW order $O > 0$, the currents $J_{\alpha\sigma}^\parallel > 0$, $J_\alpha^\perp > 0$, and $J_\sigma^\perp = 0$, the corresponding phase is the ODW Vortex I state. When $V_{\text{ex}}/t \in [0.77, 8]$, the SDW order $S = 0$, the ODW order $O = 0$, the currents $J_{\alpha\sigma}^\parallel > 0$, $J_\alpha^\perp = 0$, and $J_\sigma^\perp = 0$, the corresponding phase is the Meissner state.

According to Hamiltonian (5), there are three different interaction parameters U , V_{ex} and U_0 . It is straightforward to see that the CDW order is favored for the attractive interactions ($U < 0$, $U_0 < 0$, $V_{\text{ex}} < 0$);

and that the SDW order is favored for the attractive inter-orbital spin-preserving interaction ($U_0 < 0$). This is because the CDW order can decrease the interaction energy of all the attractive on-site interactions. While the SDW order mainly decreases the energy of the attractive inter-orbital spin-preserving interactions. These are consistent with previous studies on the SU(2) ladder systems [41, 43]. Note that for the phase diagrams in Figs. 4 and 6, we have fixed $U_0 = V_{\text{ex}} + U$. In the phase diagrams, the CDW state becomes unstable against the Vortex II state when U is not sufficiently negative. Apparently, the competition between the CDW and the SDW orders is driven by the interactions associated with U and U_0 , which is eventually determined by the relative values of U and V_{ex} . On the other hand, the emergence of the ODW order in Fig. 6 can be understood as a configuration in which the repulsive energies are minimized in the case of $U > 0$ and $U_0 > 0$. A subtlety here is the impact of the magnetic flux in the x - α plane on the density ordered phases. From numerical analysis, we see that an increase of magnetic flux can lead to a stronger competition between different density-ordered phases, which gives rise to a richer phase diagram. In any case, we emphasize that the exotic Vortex II state with the SDW order is always robust in the negative U_0 limit.

VI. DETECTION

Given the rich phase diagram discussed above, a natural question is how to detect them experimentally. In general, the different phases of the system are characterized by their chiral edge currents as well as the density correlations in different channels such as CDW, ODW and SDW. Here, the density orders can be probed by state-selective measurements of density distributions. While the CDW order can be identified by oscillations of the total density distribution from site to site, the ODW and the SDW orders can be identified, respectively, by oscillations of the density distribution of a given orbital ($|g\rangle$ or $|e\rangle$) or of a given spin ($|\uparrow\rangle$ or $|\downarrow\rangle$). For the detection of the Meissner and the vortex states, one can in principle follow the approach in Ref. [30], where, by projecting the wave function into isolated double wells along each leg, the chiral currents can be calculated from the oscillatory density dynamics in the double wells. The vortex state can be identified either from the variation of the chiral currents, as the maximum of the chiral currents

appear at the phase boundary between the Meissner and the vortex states [see Figs. 4(a) and 6(a)]. Alternatively, one should also identify the Vortex I and the Vortex II states, respectively, from the relative phase between the oscillations of different orbital and spin states. The relative phase should be π in the case of the Meissner state, and smaller than π in the case of the vortex states [30].

VII. CONCLUSION

We show that by implementing synthetic SOC in alkaline-earth-like atoms, one naturally realizes multiple two-leg ladders with uniform synthetic flux. As interactions couple different ladders together, the system features a rich phase diagram. In particular, we demonstrate the existence of an interaction-induced vortex state, which possesses SDW in the spin channel. The different phases can be experimentally detected based on their respective properties. As many phases in the phase diagram simultaneously feature density order and edge or bulk currents, a potential experimental challenge lies in the efficient detection of the various phases. This is particularly so for the exotic interaction-induced Vortex II state, whose SDW order as well as the bulk currents along SD σ require spin-selective detections. Nevertheless, with the state of the art quantum control over the clock states in alkaline-earth-like atoms, we expect that these challenges can be overcome with existing experimental techniques. Our results reveal the impact of interactions on spin-orbit coupled systems, and are particularly relevant to the on-going exploration of spin-orbit coupled optical lattice clocks.

Acknowledgments

This work is supported partly by the National Key R&D Program of China under Grants No. 2017YFA0304203 and No. 2016YFA0301700; the NKBRP under Grant No. 2013CB922000; the NSFC under Grants No. 60921091, No. 11374283, No. 11434007, No. 11422433, No. 11522545, and No. 11674200; “Strategic Priority Research Program(B)” of the Chinese Academy of Sciences under Grant No. XDB01030200; the PCSIRT under Grant No. IRT13076; the FANEDD under Grant No. 201316; SFSSSP; OYTPSP; and SSCC. J.-S. P. acknowledges support from National Postdoctoral Program for Innovative Talents of China under Grant No. BX201700156.

-
- [1] M. Z. Hasan and C. L. Kane, Topological insulators, *Rev. Mod. Phys.* **82**, 3045 (2010).
 [2] X.-L. Qi and S.-C. Zhang, Topological insulators and superconductors, *Rev. Mod. Phys.* **83**, 1057 (2011).

- [3] J. Alicea, New directions in the pursuit of Majorana fermions in solid state systems, *Rep. Prog. Phys.* **75**, 076501 (2012).
 [4] Y.-J. Lin, K. Jiménez-García, and I. B. Spielman, Spin-

- orbit-coupled Bose-Einstein condensates, *Nature (London)* **471**, 83 (2011).
- [5] P. Wang, Z.-Q. Yu, Z. Fu, J. Miao, L. Huang, S. Chai, H. Zhai, and J. Zhang, Spin-Orbit Coupled Degenerate Fermi Gases, *Phys. Rev. Lett.* **109**, 095301 (2012).
- [6] L. W. Cheuk, A. T. Sommer, Z. Hadzibabic, T. Yefsah, W. S. Bakr, and M.W. Zwierlein, Spin-Injection Spectroscopy of a Spin-Orbit Coupled Fermi Gas, *Phys. Rev. Lett.* **109**, 095302 (2012).
- [7] Z. Meng, L. Huang, P. Peng, D. Li, L. Chen, Y. Xu, C. Zhang, P. Wang, and J. Zhang, Experimental Observation of a Topological Band Gap Opening in Ultracold Fermi Gases with Two-Dimensional Spin-Orbit Coupling, *Phys. Rev. Lett.* **117**, 235304 (2016).
- [8] L. Huang, Z. Meng, P. Wang, P. Peng, S.-L. Zhang, L. Chen, D. Li, Q. Zhou, and J. Zhang, Experimental realization of two-dimensional synthetic spin-orbit coupling in ultracold Fermi gases, *Nat. Phys.* **12**, 540 (2016).
- [9] Z. Wu, L. Zhang, W. Sun, X.-T. Xu, B.-Z. Wang, S.-C. Ji, Y. Deng, S. Chen, X.-J. Liu, and J.-W. Pan, Realization of two-dimensional spin-orbit coupling for Bose-Einstein condensates, *Science* **354**, 83 (2016).
- [10] L. F. Livi, G. Cappellini, M. Diem, L. Franchi, C. Clivati, M. Frittelli, F. Levi, D. Calonico, J. Catani, M. Inguscio, and L. Fallani, Synthetic Dimensions and Spin-Orbit Coupling with an Optical Clock Transition, *Phys. Rev. Lett.* **117**, 220401 (2016).
- [11] S. Kolkowitz, S. L. Bromley, T. Bothwell, M. L. Wall, G. E. Marti, A. P. Koller, X. Zhang, A. M. Rey, J. Ye, Spin-orbit-coupled fermions in an optical lattice clock, *Nature (London)* **542**, 66 (2017).
- [12] V. Galitski and I. B. Spielman, Spin-orbit coupling in quantum gases, *Nature (London)* **494**, 49 (2013).
- [13] N. Goldman, G. Juzeliūnas, P. Öhberg, and I. B. Spielman, Light-induced gauge fields for ultracold atoms, *Rep. Prog. Phys.* **77**, 126401 (2014).
- [14] X. Zhou, Y. Li, Z. Cai, and C. Wu, Unconventional states of bosons with the synthetic spin-orbit coupling, *J. Phys. B: At. Mol. Opt. Phys.* **46**, 134001 (2014).
- [15] H. Zhai, Degenerate quantum gases with spin-orbit coupling: a review, *Rep. Prog. Phys.* **78**, 026001 (2015).
- [16] W. Yi, W. Zhang, and X. Cui, Pairing superfluidity in spin-orbit coupled ultracold Fermi gases, *Sci. China: Phys. Mech. Astron.* **58**, 014201 (2015).
- [17] J. Zhang, H. Hu, X. J. Liu, and H. Pu, Fermi gases with synthetic spin-orbit coupling, *Ann. Rev. Cold At. Mol.* **2**, 81 (2015).
- [18] Y. Xu and C. Zhang, Topological Fulde Ferrell superfluids of a spin orbit coupled Fermi gas, *Int. J. Mod. Phys. B* **29**, 1530001 (2015).
- [19] O. Boada, A. Celi, J. I. Latorre, and M. Lewenstein, Quantum Simulation of an Extra Dimension, *Phys. Rev. Lett.* **108**, 133001 (2012).
- [20] A. Celi, P. Massignan, J. Ruseckas, N. Goldman, I. B. Spielman, G. Juzeliūnas, and M. Lewenstein, Synthetic Gauge Fields in Synthetic Dimensions, *Phys. Rev. Lett.* **112**, 043001 (2014).
- [21] O. Boada, A. Celi, J. Rodríguez-Laguna, J. I. Latorre, and M. Lewenstein, Quantum simulation of non-trivial topology, *New J. Phys.* **17**, 045007 (2015).
- [22] E. Anisimovas, M. Račiūnas, C. Sträter, A. Eckardt, I. B. Spielman, and G. Juzeliūnas, Semisynthetic zigzag optical lattice for ultracold bosons, *Phys. Rev. A* **94**, 063632 (2016).
- [23] B. K. Stuhl, H.-I. Lu, L. M. Aycock, D. Genkina, and I. B. Spielman, Visualizing edge states with an atomic Bose gas in the quantum Hall regime, *Science* **349**, 1514 (2015).
- [24] M. Mancini, G. Pagano, G. Cappellini, L. Livi, M. Rider, J. Catani, C. Sias, P. Zoller, M. Inguscio, M. Dalmonte, and L. Fallani, Observation of chiral edge states with neutral fermions in synthetic Hall ribbons, *Science* **349**, 1510 (2015).
- [25] X. Cui, B. Lian, T.-L. Ho, B. L. Lev, and H. Zhai, Synthetic gauge field with highly magnetic lanthanide atoms, *Phys. Rev. A* **88**, 011601 (2013).
- [26] N. Q. Burdick, Y. Tang, and B. L. Lev, Long-lived spin-orbit-coupled degenerate dipolar Fermi gas, *Phys. Rev. X* **6**, 031022 (2016).
- [27] M. L. Wall, A. P. Koller, S. Li, X. Zhang, N. R. Cooper, J. Ye, and A. M. Rey, Synthetic Spin-Orbit Coupling in an Optical Lattice Clock, *Phys. Rev. Lett.* **116**, 035301 (2016).
- [28] E. Orignac and T. Giamarchi, Meissner effect in a bosonic ladder, *Phys. Rev. B* **64**, 144515 (2001).
- [29] A. Petrescu and K. L. Hur, Bosonic Mott Insulator with Meissner Currents, *Phys. Rev. Lett.* **111**, 150601 (2013).
- [30] M. Atala, M. Aidelsburger, M. Lohse, J. T. Barreiro, B. Paredes, and I. Bloch, Observation of chiral currents with ultracold atoms in bosonic ladders, *Nat. Phys.* **10**, 588 (2014).
- [31] M. Piraud, F. Heidrich-Meisner, I. P. McCulloch, S. Greschner, T. Vekua, and U. Schollwöck, Vortex and Meissner phases of strongly interacting bosons on a two-leg ladder, *Phys. Rev. B* **91**, 140406(R) (2015).
- [32] S. S. Natu, Bosons with long-range interactions on two-leg ladders in artificial magnetic fields, *Phys. Rev. A* **92**, 053623 (2015).
- [33] F. Kolley, M. Piraud, I. P. McCulloch, U. Schollwöck, and F. Heidrich-Meisner, Strongly interacting bosons on a three-leg ladder in the presence of a homogeneous flux, *New J. Phys.* **17**, 092001 (2015).
- [34] S. Greschner, M. Piraud, F. Heidrich-Meisner, I. P. McCulloch, U. Schollwöck, and T. Vekua, Spontaneous Increase of Magnetic Flux and Chiral-Current Reversal in Bosonic Ladders: Swimming against the Tide, *Phys. Rev. Lett.* **115**, 190402 (2015).
- [35] S. Greschner, M. Piraud, F. Heidrich-Meisner, I. P. McCulloch, U. Schollwöck, and T. Vekua, Symmetry-broken states in a system of interacting bosons on a two-leg ladder with a uniform Abelian gauge field, *Phys. Rev. A* **94**, 063628 (2016).
- [36] A. K. Geim, S. V. Dubonos, J. G. S. Lok, M. Henini, and J. C. Maan, Paramagnetic Meissner effect in small superconductors, *Nature (London)* **396**, 144 (1998).
- [37] X. Zhang, M. Bishof, S. L. Bromley, C. V. Kraus, M. S. Safronova, P. Zoller, A. M. Rey, and J. Ye, Spectroscopic observation of SU(N)-symmetric interactions in Sr orbital magnetism, *Science* **345**, 1467 (2014).
- [38] G. Cappellini, M. Mancini, G. Pagano, P. Lombardi, L. Livi, M. Siciliani de Cumis, P. Cancio, M. Pizzocaro, D. Calonico, F. Levi, C. Sias, J. Catani, M. Inguscio, and L. Fallani, Direct Observation of Coherent Interorbital Spin-Exchange Dynamics, *Phys. Rev. Lett.* **113**, 120402 (2014); *ibid* **114**, 239903 (2015).
- [39] F. Scazza, C. Hofrichter, M. Höfer, P. C. De Groot, I. Bloch, and S. Fölling, Observation of two-orbital spin-

- exchange interactions with ultracold SU(N)-symmetric fermions, *Nat. Phys.* **10**, 779 (2014); *ibid* **11**, 514 (2015).
- [40] K. Kobayashi, M. Okumura, Y. Ota, S. Yamada, and M. Machida, Nontrivial Haldane phase of an atomic two-component Fermi gas trapped in a 1D optical lattice, *Phys. Rev. Lett.* **109**, 235302 (2012).
- [41] H. Nonne, M. Moliner, S. Capponi, P. Lecheminant, and K. Totsuka, Symmetry-protected topological phases of alkaline-earth cold fermionic atoms in one dimension, *Europhys. Lett.* **102**, 37008 (2013).
- [42] K. Duivendoorn and T. Quella, Topological phases of spin chains, *Phys. Rev. B* **87**, 125145 (2013).
- [43] V. Bois, S. Capponi, P. Lecheminant, M. Moliner, and K. Totsuka, Phase diagrams of one-dimensional half-filled two-orbital SU(N) cold fermion systems, *Phys. Rev. B* **91**, 075121 (2015).
- [44] A. Roy and T. Quella, Chiral Haldane phases of SU(N) quantum spin chains in the adjoint representation, arXiv: 1512.05229.
- [45] V. Bois, P. Fromholz, and P. Lecheminant, One-dimensional two-orbital SU(N) ultracold fermionic quantum gases at incommensurate filling: A low-energy approach, *Phys. Rev. B* **93**, 134415 (2016).
- [46] S. Capponi, P. Lecheminant, and K. Totsuka, Phases of one-dimensional SU(N) cold atomic Fermi gases—From molecular Luttinger liquids to topological phases, *Ann. Phys.* **367**, 50 (2016).
- [47] X. Zhou, J.-S. Pan, Z.-X. Liu, W. Zhang, W. Yi, G. Chen, and S. Jia, Symmetry-protected topological states for interacting fermions in alkaline-earth-like atoms, arXiv: 1612.08880.
- [48] F. Iemini, L. Mazza, L. Fallani, P. Zoller, R. Fazio, and M. Dalmonte, Majorana Quasiparticles Protected by \mathbb{Z}_2 Angular Momentum Conservation, *Phys. Rev. Lett.* **118**, 200404 (2017).
- [49] S. R. White, Density matrix formulation for quantum renormalization groups, *Phys. Rev. Lett.* **69**, 2863 (1992).
- [50] U. Schollwöck, The density-matrix renormalization group, *Rev. Mod. Phys.* **77**, 259 (2005).
- [51] R. Zhang, Y. Cheng, H. Zhai, and P. Zhang, Orbital Feshbach Resonance in Alkali-Earth Atoms, *Phys. Rev. Lett.* **115**, 135301 (2015).
- [52] M. Höfer, L. Riegger, F. Scazza, C. Hofrichter, D. R. Fernandes, M. M. Parish, J. Levinsen, I. Bloch, and S. Fölling, Observation of an Orbital Interaction-Induced Feshbach Resonance in ^{173}Yb , *Phys. Rev. Lett.* **115**, 265302 (2015).
- [53] G. Pagano, M. Mancini, G. Cappellini, L. Livi, C. Sias, J. Catani, M. Inguscio, and L. Fallani, Strongly Interacting Gas of Two-Electron Fermions at an Orbital Feshbach Resonance, *Phys. Rev. Lett.* **115**, 265301 (2015).
- [54] M. Olshanii, Atomic Scattering in the Presence of an External Confinement and a Gas of Impenetrable Bosons, *Phys. Rev. Lett.* **81**, 938 (1998).
- [55] R. Zhang, D. Zhang, Y. Cheng, W. Chen, P. Zhang, and H. Zhai, Kondo effect in alkaline-earth-metal atomic gases with confinement-induced resonances, *Phys. Rev. A* **93**, 043601 (2016).
- [56] J.-S. Pan, X.-J. Liu, W. Zhang, W. Yi, and G.-C. Guo, Topological Superradiant States in a Degenerate Fermi Gas, *Phys. Rev. Lett.* **115**, 045303 (2015).
- [57] L. Zhou and X. Cui, Spin-orbit coupled ultracold gases in optical lattices: High-band physics and insufficiency of tight-binding models, *Phys. Rev. B* **92**, 140502(R) (2015).
- [58] J.-S. Pan, W. Zhang, W. Yi, and G.-C. Guo, Bose-Einstein condensate in an optical lattice with Raman-assisted two-dimensional spin-orbit coupling, *Phys. Rev. A* **94**, 043619 (2016).
- [59] S. Barbarino, L. Taddia, D. Rossini, L. Mazza, and R. Fazio, Magnetic crystals and helical liquids in alkaline-earth fermionic gases, *Nat. Commun.* **6**, 8134 (2015).